MODELING ROCK BOLT REINFORCEMENT BY USING THE PARTICULATE INTERFACE MODEL OF DEM

Meng-Chia Weng [1*], Fu-Shu Jeng [2], Chia-Chi Chiu [3], and Yu-Cheng Lin [2]

ABSTRACT

Rock bolt is widely used to stabilize suspended rock blocks at an excavation section, reinforce rock mass, and reduce displacement along rock joints. To simulate the rock bolt behavior in discrete element method (DEM), this study proposed a rock bolt model based on discrete element method software Particle Flow Code (PFC), which simulates the interfaces between the rock bolt and surrounding rock mass using the particulate interface model with high strength and stiffness. On the basis of the proposed model, the DEM simulation can effectively install a series of rock bolts at particular positions to form a support system. The proposed model was verified using laboratory pull-out and shear tests. A series of tunnel cases were further simulated to compare the difference among the displacement distributions of the tunnel under different rock bolt configurations. The simulation results showed that the proposed model can simulate rock bolt functions on tunnel excavation. Furthermore, the results showed that increasing the length and number of rock bolts increases the reinforced effect; however, as the length and number of rock bolts increased to an upper bound value, a limited increment was observed in the reinforced effect. The proposed model provides a useful tool to simulate the rock bolt system for tunnel engineering.

Key words: Discrete element method, rock bolt, particulate interface model, tunnel.

1. INTRODUCTION

Rock bolt is one of the major support elements of tunnel engineering and is widely adopted in the new Austrian tunneling method (NATM). A steel rebar is generally fixed into rock mass by grouting and used as a rock bolt. It is used to stabilize suspended rock blocks at an excavation section, reinforce the rock mass, and reduce displacement along rock joints. To investigate the interaction behavior between a rock bolt and surrounded rock, many researchers (Cook 1993; Spang and Egger 1990) have conducted a series of laboratory tests on rock bolts embedded in concrete or rocks, such as pull-out, shear, and combined pull–shear tests. According to Cook (1993), the rock bolt exhibits four possible failure modes under tensile loading, namely (1) concrete cone failure, (2) combined cone–bond failure, (3) bond failure, and (4) steel failure (Fig. 1). Spang and Egger (1990) investigated shear failure patterns between the rock bolt and rock when the specimen was under shear loading. These test results provide a valuable knowledge base for the development of analytical studies and numerical modeling of rock bolts.

In recent decades, the discrete element method (DEM) has been considerably developed and successfully employed to numerous science and engineering fields, such as powder technology, geotechnical engineering, tunneling, landslide, and mining

engineering (Chiu *et al.* 2015; Chiu *et al.* 2017; Weng *et al.* 2017). Compared with a continuum analysis, the DEM has several unique characteristics and advantages, such as the ability to simulate crack propagation, large deformation, post-peak behavior, and block movement (Weng *et al.* 2015; Wu *et al.* 2016; Lin *et al.* 2018). The DEM has been implemented in many programs, and this study employed particle flow code (PFC) software (Itasca, Inc. 2014), which is widely used in rock and geotechnical engineering. PFC is a type of particulate DEMs, which indicates that the basic element comprises a ball. To simulate the rock bolt behavior embedded in the rock using PFC, Chiu (2010) indicated two types of models that could be adopted: (1) increasing the strength of surrounding rock elements to simulate the reinforcement of rock bolts and (2) removing rock elements and installing high-strength bonded elements in a vacancy area to simulate the rock bolt. Although these two models can reflect the reinforcing effect of the bolt on the rock mass, evaluating the interaction between the bolt and rock mass is difficult and the simulated failure patterns are inconsistent with the actual patterns. In addition, the simulation of the latter model is time consuming, and installing a series of rock bolts around the excavation section is difficult because determining the position of bolt elements is challenging. Therefore, this study aimed to propose a rock bolt model based on the specified rock bolt–rock interface concept to reasonably simulate the interaction between the bolt and rock mass. In the simulation based on the proposed model, a series of rock bolts can be effectively installed at particular positions to form a support system, which provides essential information for engineering design.

The proposed rock bolt model includes two parts: the bolt body and interface. To deal with the interaction on the interface between the rock bolt and rock mass, the particulate interface model (PIM) was adopted (Chiu and Weng 2019). The PIM was originally developed for the simulation of the joint, that is, for the discontinuity behavior, and it ensures that particles at the joint

[1] Professor (corresponding author), Department of Civil Engineering, National Chiao Tung University, Hsinchu, Taiwan (e-mail: mcweng@nctu.edu.tw).

[2] Professor, Department of Civil Engineering, National Taiwan University, Taipei, Taiwan.

[3*] Assistant Professor, Institute of Mineral Resources Engineering, National Taipei University of Technology, Taipei, Taiwan.

(a) Concrete cone failure   (b) Combined cone-bond failure   (c) Bond failure

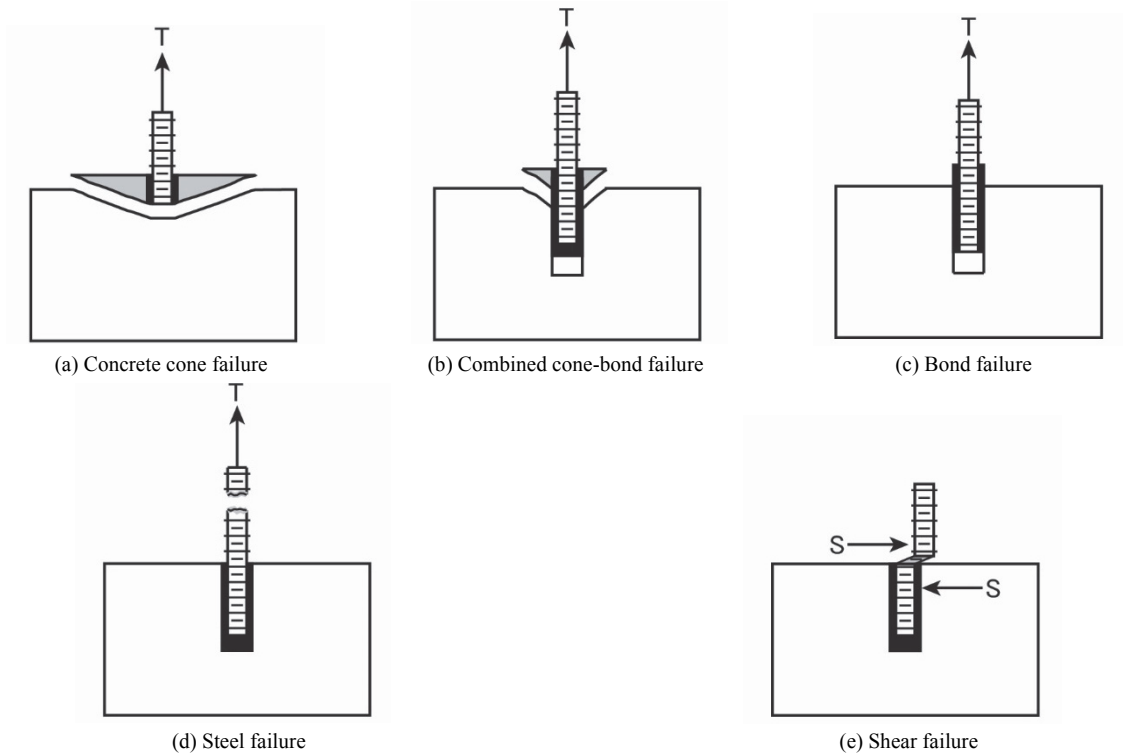(d) Steel failure   (e) Shear failure

Fig. 1   Five possible failure modes of rock bolts under tensile and shear loading. (a) concrete cone failure, (b) combined cone-bond failure, (c) bond failure, (d) steel failure, and (e) shear failure (after Cook 1993; Spang and Egger 1990)

surface, which experience a relative slip, slide on the specified joint face and not along the particle surface (Fig. 2). Numerous applications have been derived from the PIM, such as rock sliding and seepage in the rock joint. The aforementioned studies have revealed the usefulness of the PIM for investigating the effects of interfaces in rock mechanics. The interaction between a bolt and rock masses can be considered as an interface problem. In contrast to the low strength and stiffness of a joint, the interface between a bolt and rock masses exhibits high strength and stiffness.

Therefore, this study modified the original PIM to create specified interfaces with high strength and stiffness. The proposed model was first validated using laboratory tensile and shear tests. A series of tunnel cases were then simulated to compare the difference among the displacement distributions of the tunnel under different rock bolt configurations. The study performed a two-dimensional analysis, in which the rock bolt system can be regarded as installation in equal spacing along the longitudinal direction of the tunnel.
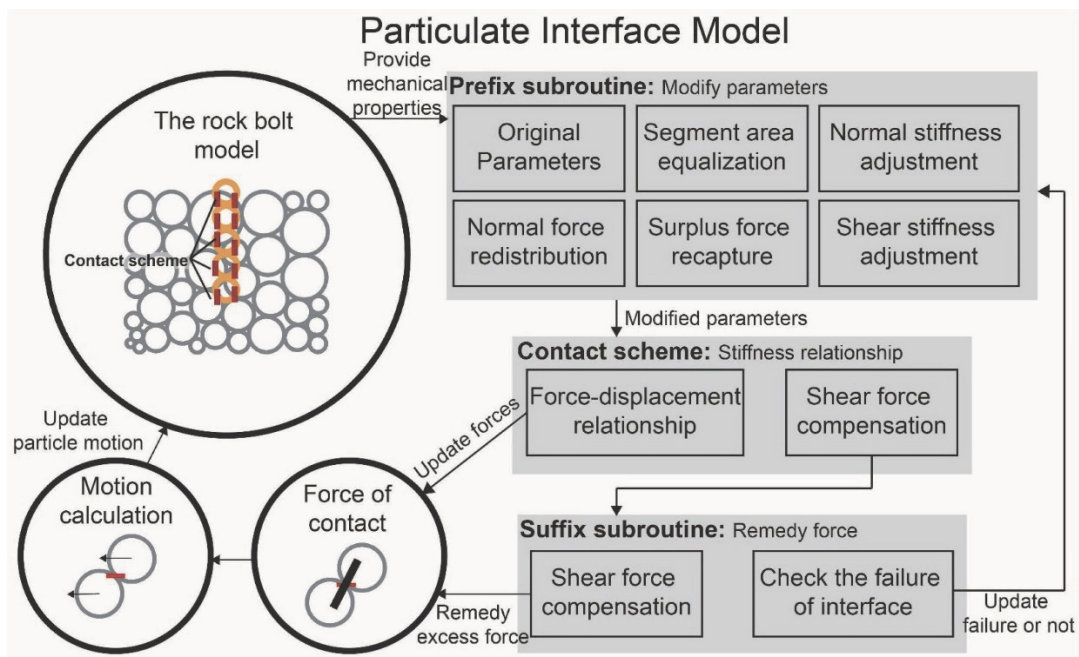

Fig. 2   Schematic illustration of the particulate interface model (PIM)

2. ROCK BOLT BEHAVIOR

2.1 Failure Mode

According to Cook (1993), Spang and Egger (1990), and Chen (2014), the rock bolt exhibits five possible failure modes under tensile and shear loading (Fig. 1). The details of rock bolt failure modes are described in the following section, and they provide a reference for the following simulation of the rock bolt behavior.

1. Concrete cone failure (Fig. 1(a)): Luke *et al.* (1985) indicated that when the embedment depth of the rock bolt is shallow, the concrete cone failure is commonly observed. The cone failure initiates at the end of the rock bolt and propagates to the free surface.

2. Combined cone–bond failure (Fig. 1(b)): As the embedment depth increases, the failure mode changes into a combined cone–bond failure. This failure includes a bond failure along the deeper part of the bolt, with a shallow cone at the top of the bolt.

3. Bond failure (Fig. 1(c)): The bond failure occurs along the interface between the bolt and rock, which is caused by the insufficient strength of the grout, low friction of rebar, or deficiency of the bonding surface.

4. Steel failure (Fig. 1(d)): The failure develops at the rebar when the tensile stress is higher than the ultimate strength of the rebar.

5. Shear failure (Fig. 1(e)): When the shear stress is higher than the ultimate strength of the rebar, the rebar is sheared off.

2.2 Pull-Out Behavior

After the bolt is embedded in the rock mass around a tunnel section, the external force primarily results in the tensile stress on the bolt. Therefore, many researchers have focused on the pull-out behavior of the rock bolt and proposed the associated theories for predicting the force–displacement relation and stress distribution of the rock bolt (Thenevin *et al.* 1985; Li and Stillborg 1999; Cai *et al.* 2004). Collins *et al.* (1989) conducted a series of pull-out and fatigue tests to study the rock bolt behavior with different bonding materials, bolt types, and surrounding materials. In total, 178 specimens were evaluated. Figure 3 shows a typical load–displacement curve of the pull-out test. The length and height of the concrete specimen were 800 and 500 mm, respectively, and the uniaxial compressive strength was 38 MPa. A rock bolt with a diameter of 10 mm was embedded in the central part of concrete. The embedment depth of the bolt was 200 mm. In Fig. 3, the ultimate pull-out load was 138 kN at a displacement of 0.004 m. The failure mode was classified as the combined cone–bond failure. This study used the test results to validate the proposed model in Section 4.

2.3 Shear Behavior

Spang (1988) conducted direct shear tests to study the shear behavior of the rock bolt embedded in concrete. The specimen comprised a rock bolt and two concrete blocks, and a rock bolt with 8-mm diameter was vertically installed between these two blocks (Fig. 4). The length and height of each concrete block were 100 and 50 mm, respectively, and the uniaxial compressive strength was 40 MPa. Figure 4 shows the shear force–displacement curve of the direct shear test. The ultimate shear load was 40 kN at a displacement of 0.015 m. The test result was used to validate the simulated shear behavior of the proposed model in Section 5.
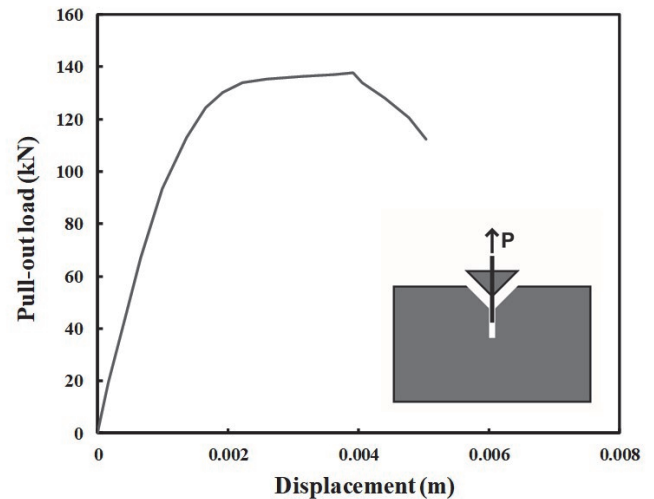

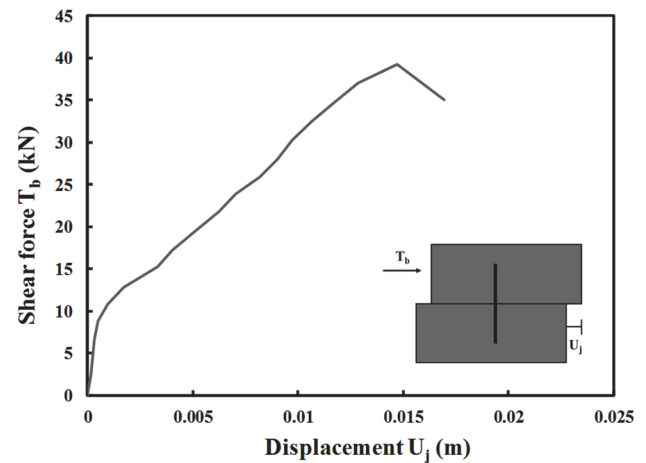**Fig. 3 A pull-out test result of the rock bolt (after Collins *et al.* 1989)**

Fig. 4 A direct shear test result of the rock bolt (after Spang 1988)

3. ROCK BOLT MODEL OF THE DEM

3.1 Concept of the Rock Bolt Model

The proposed rock bolt model includes two parts: the bolt body and interface (Fig. 5). The bolt body is composed of raw bonded ball elements, and the installation of rock bolts is directly installed on the specified position without removing rock mass elements. It makes the rock bolts easily to set up on specified positions, and the rearrangement of particles is unnecessary (Fig. 5). With the use of the bolt installation method, the interfaces between the rock bolt and surrounding rock mass were simulated using the PIM. The PIM ensures that particles at the joint surface, which experience a relative slip, slide on the specified joint face and not along the particle surface, and thus, it can eliminate roughness caused by the arrangement of particles on the joint face. On the basis of the features of the PIM, this study simulated the high-strength interaction between the rock bolt and rock mass.

Chiu and Weng (2019a) indicated that the algorithm of the PIM involves a prefix subroutine, a suffix subroutine and a contact model (Fig. 2). Six modifications are deployed in the PIM to correct the simulation results, which are (1) segment area equalization, (2) shear stiffness adjustment, (3) surplus force recapture, (4) shear
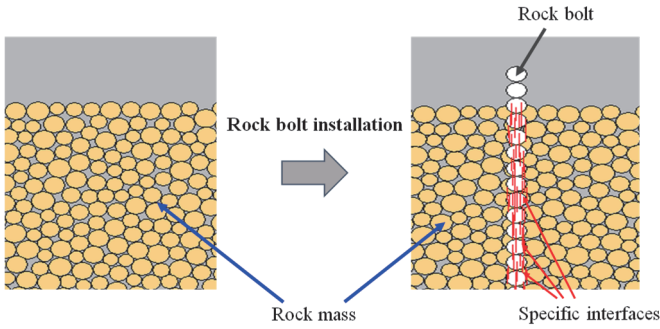
Fig. 5 Schematic illustration of the proposed rock bolt model

force compensation, (5) normal force redistribution, and (6) normal stiffness adjustment. These modifications will be elucidated in the following sections. More detailed information and algorithms associated with the PIM can be found in two recent studies (Chiu and Weng 2019a; Chiu and Weng 2019b).

On the basis of the PIM, the force on the interface is calculated as follows:

$$F_{n,sj} := F_{n,sj} + k_{n,sj}\, A_{sj}\, \Delta U_n^e \tag{1}$$

$$\mathbf{F}'_{s,sj} := \mathbf{F}_{s,sj} - k_{s,sj}\, A_{sj}\, \Delta \mathbf{U}_s^e \tag{2}$$

where $F_{n,sj}$ and ΔU_n^e are the normal force acting on an interface plane and normal displacement in the unbonded part of the interface, respectively. $\mathbf{F}'_{s,sj}$ is the shear force vector acting on the interface plane. The bold font indicates that the term is in a vector form. $\Delta \mathbf{U}_s^e$ and A_{sj} are the shear displacement vector of the interface and the area of the interface cross section, respectively.

For an interface, if $|\mathbf{F}'_{s,sj}| \le F^*_{s,sj}$, where $F^*_{s,sj} = \mu F_{n,sj} + c_{sj}$, then the resistant shear force $|\mathbf{F}_{s,sj}|$ is as follows:

$$|\mathbf{F}_{s,sj}| = |\mathbf{F}'_{s,sj}| \tag{3}$$

where μ and c_{sj} are the coefficient of friction and cohesion of interface, respectively.

Otherwise, sliding is assumed to occur, and the resistant shear force is limited as follows:

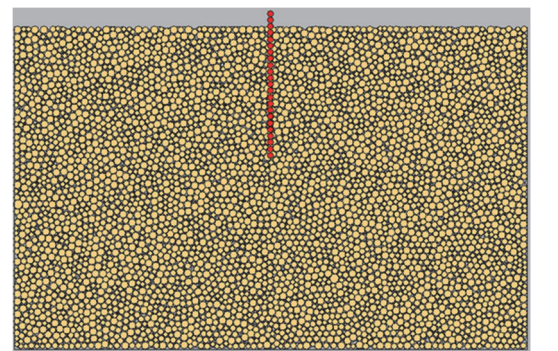$$|\mathbf{F}_{s,sj}| = F^*_{s,sj} \tag{4}$$

3.2 Required Parameters of the Model

The proposed rock bolt model required 10 micro-parameters. Among these parameters, six parameters were for the bolt body, namely the normal stiffness of the ball, shear stiffness of the ball, normal bonding stiffness, shear bonding stiffness, normal bonding strength, and shear bonding strength, listed in Table 1. Four parameters were for the interface, namely friction angle ϕ_{sj}, cohesion c_{sj}, interface normal stiffness $k_{n,sj}$, and interface shear stiffness $k_{s,sj}$. If we assume that the rock bolt body is sufficiently strong, the steel failure could be avoided. Then, four parameters of the rock bolt body, namely the normal stiffness of the ball, shear stiffness of the ball, normal bonding strength, and shear bonding strength, exhibit a slight influence on the rock bolt behavior and can have a considerably high value. The remaining parameters could be determined through back analysis by comparing the simulation with the results of laboratory tests. To verify the proposed model, three tests, namely the pull-out test and two shear tests, are simulated in the following sections.
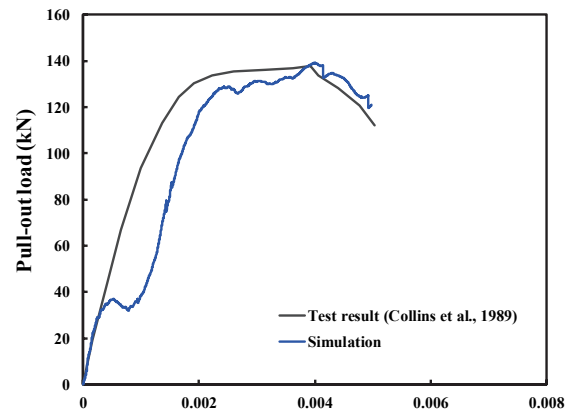
4. VERIFICATION WITH THE PULL-OUT TEST
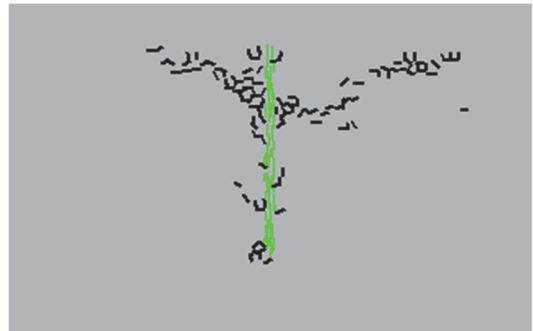
4.1 Pull-Out Test

Refeering back to Section 2.2 for the pull-out test, to evaluate the tensile performance of the rock bolt model, this study simulated the result of the pull-out test (Collins *et al.* 1989). To simplify the computation, the two-dimensional analysis was conducted. The study first established a concrete specimen of the DEM according to the suggested procedure of Potyondy and Cundall (2004). The length and height of the concrete specimen were 800 and 500 mm, respectively. The specimen comprised 5680 ball elements, and the average diameter of the ball elements was 10 mm. The stiffness of the ball and parallel bond was determined according to Potyondy and Cundall (2004), and the simulated uniaxial compressive strength was 38 MPa, which was consistent with the actual specimen. A rock bolt with a diameter of 10 mm was installed in the specimen with a depth of 200 mm (Fig. 6(a)). Table 1 presents the

(a) DEM model

(b) Force-displacement curve

(c) Crack distribution

Fig. 6 Simulation and actual results of a pull-out test of the rock bolt

Table 1   Parameters of the rock bolt model for pull-out and direct shear tests

Parameters		Pull-out test	Shear test
Bolt size (mm)		10	8
Bolt body	Density g (kg/m^3)	2800	2800
	Normal stiffness of parallel bond $\overline{k}_n$ (N/m^3)	9×10^{13}	1.5×10^{13}
	Shear stiffness of parallel bond $\overline{k}_s$ (N/m^3)	5×10^{13}	9×10^{11}
	Normal strength of parallel bond (N/m^2)	5×10^{10}	7×10^{10}
	Shear strength of parallel bond (N/m^2)	2×10^{10}	1.6×10^{9}
	Normal stiffness of particle k_n (N/m)	9×10^{9}	8×10^{11}
	Shear stiffness of particle k_s (N/m)	3×10^{9}	3×10^{11}
Interface	Friction coefficient of interface	0.83	0.83
	Cohesion of interface (N/m^2)	0	0
	Normal stiffness of interface $k_{n,sj}$ (N/m^3)	9.34×10^{9}	2×10^{8}
	Shear stiffness of interface $k_{s,sj}$ (Pa/m)	7×10^{8}	9×10^{7}

material parameters and properties. To conduct the pull-out test, the top of the rock bolt was pulled out with a constant displacement rate of 0.1 mm/s. The relation between the tensile force and pull-out displacement was recorded during the process. Figure 6(b) shows the simulation and actual result of the pull-out test. The simulation results were consistent with the test results in terms of peak strength and stiffness. Although a slight force-drop discrepancy was observed in the initial stage of the force–displacement curve, it was initiated from the partial tensile failure in the rock mass near the rock bolt. Figure 6(c) shows the failure pattern after the rock bolt was pulled out. Wedge damage accompanied with tensile cracks could be observed in the concrete specimen. This damage is consistent with the results of Collins *et al.* (1989) (Fig. 3). The simulation was validated using experimental results in terms of the force–displacement curve and failure morphology.

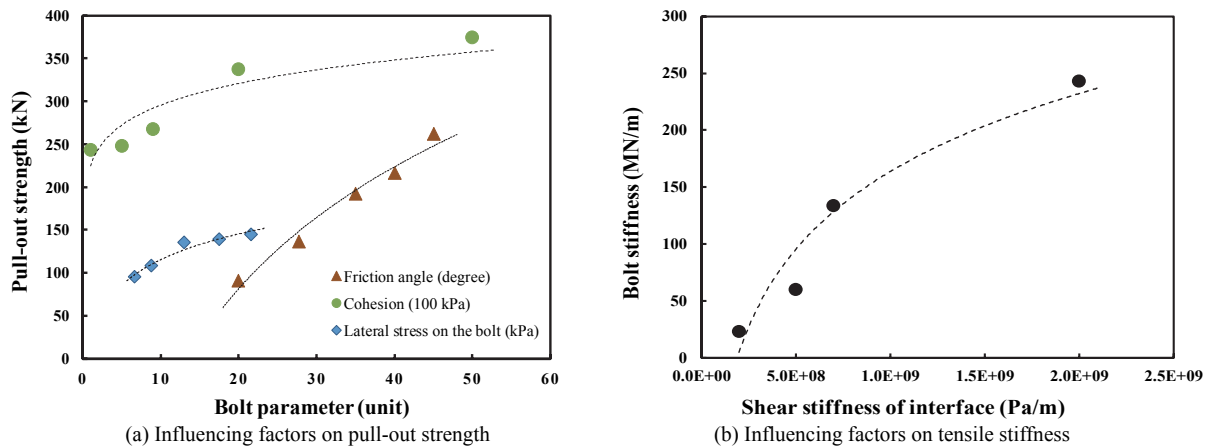### 4.2   Effects of Micro-Parameters on Tensile Resistance

This study further investigated the effect of micro-parameters on the results of the pull-out test. Figure 7 shows the effect of micro-parameters and external stress conditions on the tensile behavior during DEM simulation. Among the micro-parameters, the friction angle and cohesion of the interface exhibited a significant effect on pull-out strength (Fig. 7(a)). With the increasing friction angle and cohesion of the interface, the strength increased evidently. In addition to the micro-parameters, a lateral stress on the rock bolt is crucial. With the increasing lateral stress, which indicates an increase in the overburden depth or in situ stress, the pull-out strength simultaneously increased. For the stiffness of the pull-out test, the primary influencing factor is the shear stiffness $k_{s,sj}$ of the interface. With the increasing interface shear stiffness, strength

increased evidently (Fig. 7(b)).

5.   VERIFICATION WITH THE SHEAR TEST

5.1   Shear Test

To investigate the shear performance of the proposed model, this study simulated the results of the shear test (Spang 1988). For the direct shear test (Fig. 4), the study established two concrete blocks of the DEM based on the suggested procedure of Potyondy and Cundall (2004). The length and height of each concrete block were 100 and 50 mm, respectively, and the average diameter of the ball elements was 4 mm. The stiffness of the ball and parallel bond were determined based on Potyondy and Cundall (2004), and the simulated uniaxial compressive strength of concrete was 40 MPa, which was consistent with the actual specimen. A rock bolt with a diameter of 8 mm was then vertically installed between the two blocks (Fig. 8(a)). Table 1 presents the required material parameters and properties for the simulation. To conduct the shear test, the upper block was moved with a constant displacement rate of 0.1 mm/s. The relation between the shear force and shear displacement was obtained during the process. Figure 8(b) presents the simulation and actual results of the shear test. The simulation agreed with the test result at peak strength and stiffness at 50% strength, although a minor discrepancy was observed in the initial stage of the force–displacement curve. Figure 8(c) shows the failure pattern after the rock bolt was sheared off. The damage zone of concrete with cracks was primarily distributed near the shear plane at the backside of the rock bolt. The simulation could reflect the concrete crushing behavior after the direct shear test.

(a) Influencing factors on pull-out strength

(b) Influencing factors on tensile stiffness

Fig. 7   Influence of micro-parameters on the result of the pull-out test

(a) DEM model

(b) Force-displacement curve
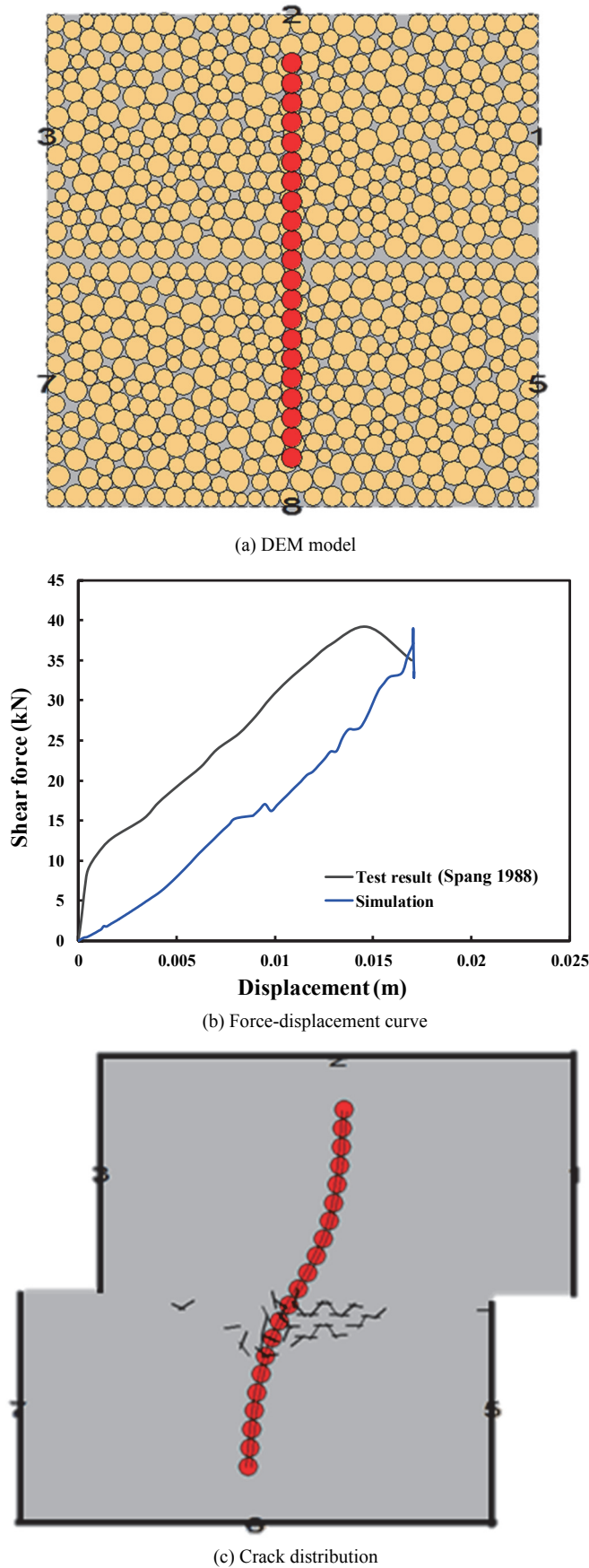

(c) Crack distribution

Fig. 8   Simulation and actual results of a direct shear test of the rock bolt

5.2   Effects of Micro-Parameters on Shear Resistance

Figure 9 shows the effect of micro-parameters on the shear behavior in DEM simulation. Among micro-parameters of the rock bolt body, normal bonding strength and shear bonding strength provide primary resistance to the external shear force. With an increase in the two bonding strengths, the shear strength of the rock bolt increased (Fig. 9(a)). For the parameters of the interface, the friction angle exhibited a significant influence on shear strength (Fig. 9(a)). For the bolt stiffness of the shear test, the primary influencing factors are the interface normal stiffness and normal bonding stiffness of the bolt body. Higher interface normal stiffness and normal bonding stiffness were associated with the higher shear stiffness of the rock bolt (Fig. 9(b)). The proposed model could not simulate the elastic–plastic behavior of the bolt, thus indicating that the bolt only exhibited brittle behavior when the shear stress reached ultimate strength. Micro stiffness parameters only affect the pre-peak macroscopic stiffness of the rock bolt and cannot generate post-peak ductile deformation. More sophisticated contact models must be adopted in the rock bolt model for considering ductile deformation after bolt yielding.
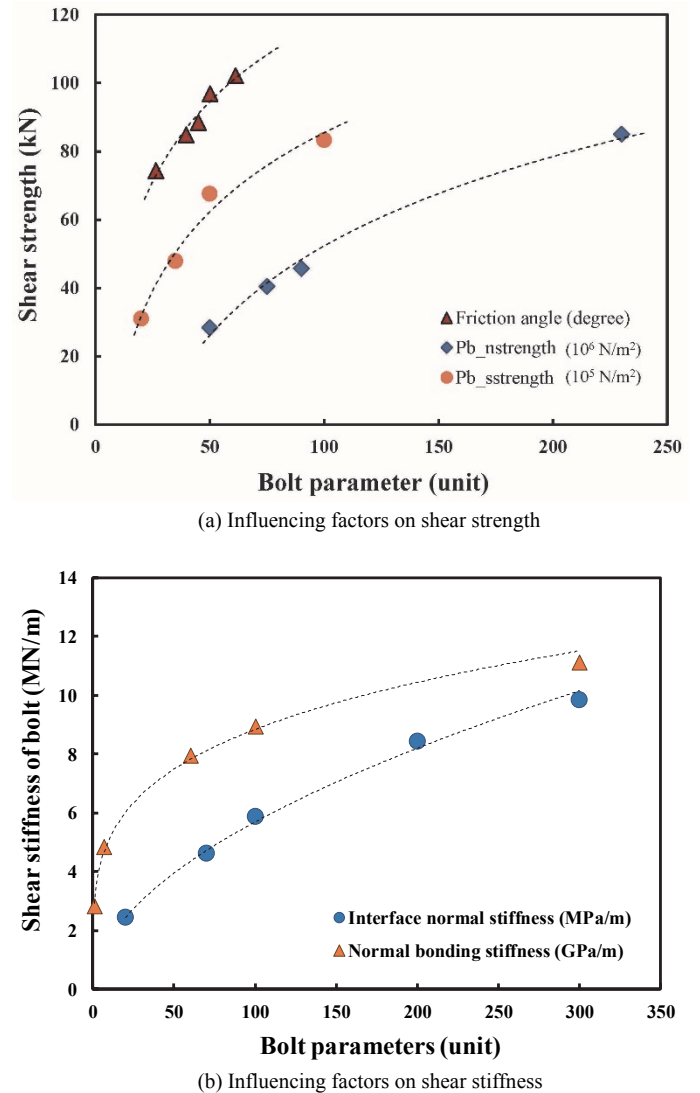

(a) Influencing factors on shear strength

(b) Influencing factors on shear stiffness

Fig. 9   Influence of micro-parameters on the result of the shear test

6. SIMULATION OF TUNNELING WITH ROCK BOLT SUPPORTS

6.1 Model Setup

This study further analyzed the performance of the numerical model to represent rock bolts in the situation of inward deformation during tunnel excavation. A recognized tunneling project in Taiwan was used as a case study. This tunnel, with a diameter of 20 m, and the overburden depth ranging from 20 m to 120 m, was constructed in the Western foothill of Taiwan. The rock mass in the tunnel was sandstone, and the property is assumed as isotropy. According to the design report (Weng *et al.* 2008; Weng *et al.* 2010), the friction angle, cohesion, Young's modulus, and Poisson's ratio of the rock mass were of 35°, 100 kPa, 200 MPa, and 0.21, respectively (Table 2).

In the analyzed case of DEM, the length and depth of the tunnel were 200 and 192 m, respectively; it comprised 11,000 ball elements, and the average diameter of the ball elements was 1 m (Fig. 10). Table 2 presents the material parameters and properties, and the simulated uniaxial compressive strength and Young's modulus were consistent with those of the rock mass. An overburden depth of the tunnel of 86 m was selected for a basic analysis. The tunnel case was analyzed using three steps: geostatic condition in the rest state, section excavation, and installation of the rock bolt system. The rock bolt system included seven bolts with a length of 8 m and were embedded at the crown and sidewall of the tunnel. Because of the absence of the actual properties of the rock bolt, the parameters of the rock bolt for the direct shear test were adopted in the tunnel analysis. Table 2 lists these parameters.

Table 2   Parameters of the Tunnel Analysis

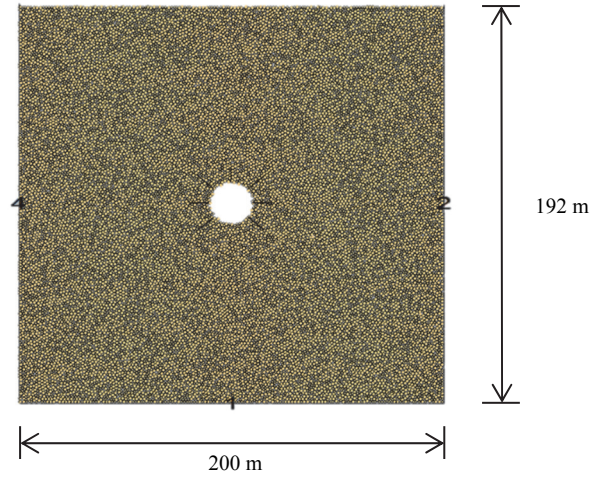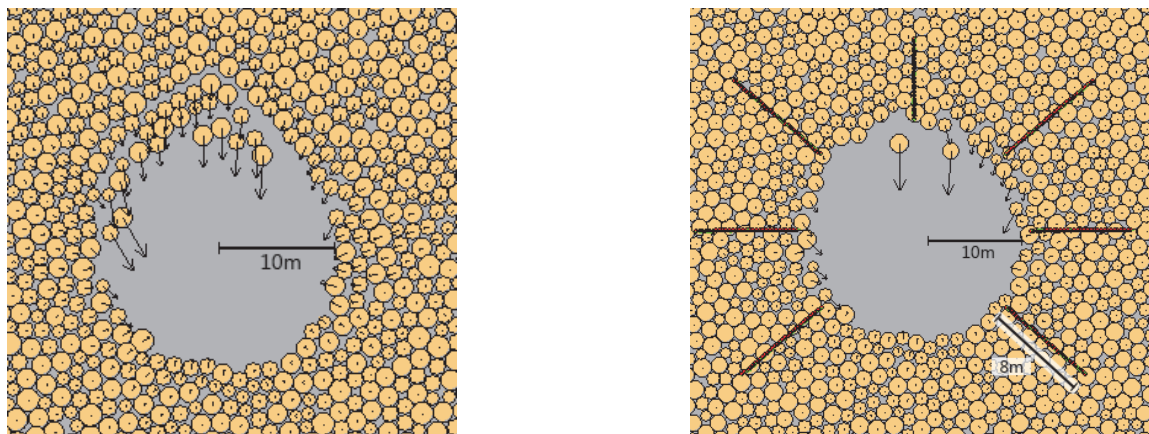| Parameters		Values
Bolt size (m)		0.3
Bolt body	Density g (kg/m³)	2800
	Normal stiffness of parallel bond $\bar{k}_n$ (N/m³)	8×10^{13}
	Shear stiffness of parallel bond $\bar{k}_s$ (N/m³)	9×10^{12}
	Normal strength of parallel bond (N/m²)	1×10^9
	Shear strength of parallel bond (N/m²)	8×10^8
	Normal stiffness of particle k_n (N/m)	7×10^9
	Shear stiffness of particle k_s (N/m)	5×10^9
Interface	Friction coefficient of interface	0.83
	Cohesion of interface (N/m²)	0
	Normal stiffness of interface $k_{n,sj}$ (N/m³)	2×10^8
	Shear stiffness of interface $k_{s,sj}$ (N/m³)	9×10^7
Rock	Average ball size (m)	1
	Density g (kg/m³)	2600
	Normal stiffness of parallel bond $\bar{k}_n$ (N/m³)	3.4×10^7
	Shear stiffness of parallel bond $\bar{k}_s$ (N/m³)	1.3×10^7
	Normal strength of parallel bond (N/m²)	3.2×10^5
	Shear strength of parallel bond (N/m²)	2×10^5
	Normal stiffness of particle k_n (N/m)	4×10^8
	Shear stiffness of particle k_s (N/m)	8×10^7
	Friction angle	35°
	Cohesion (N/m²)	1×10^5
	Young's modulus (N/m²)	2×10^8
	Poisson's ratio	0.21

Fig. 10   The analyzed tunnel case of DEM
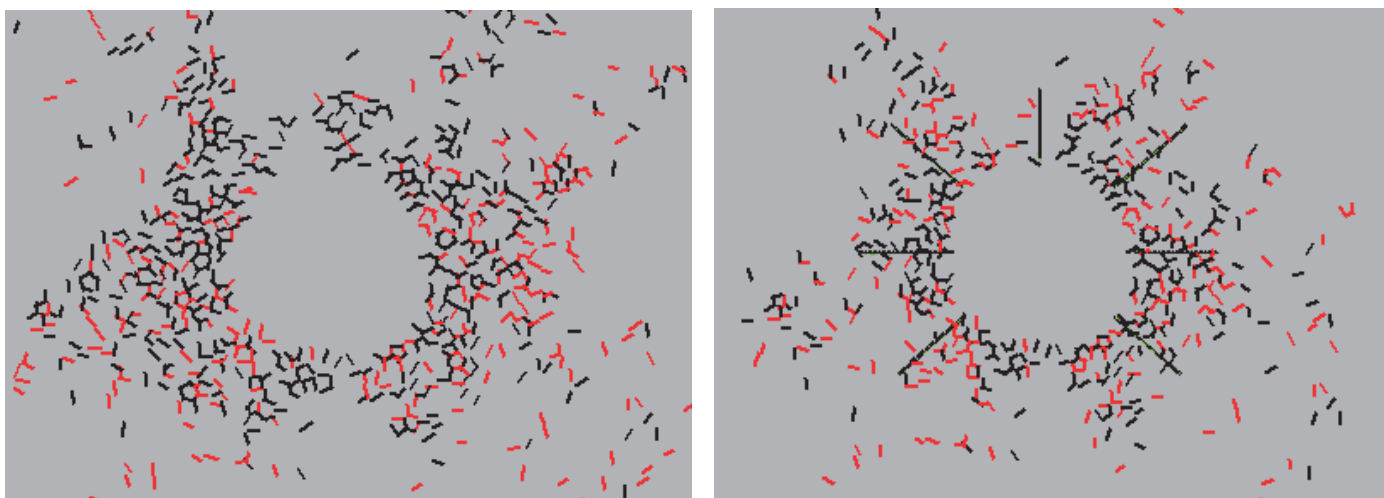
6.2 Influence of Presence of Rock Bolt Support

Two tunnel cases, excavation with and without rock bolt support, are first compared in the following section. Figure 11 shows the tunnel deformation pattern after excavation and inward displacements around the tunnel section. For the tunnel deformation pattern, the rock mass without any support exhibited large deformation at the crown and left sidewall, and a wedge failure zone was accordingly developed. Inward displacements in the failure zone were 0.38 ~ 0.60 m (Figs. 11(a) and 11(c)). After the rock bolts were installed, tunnel deformation was significantly suppressed. The average inward displacement around the tunnel was reduced to approximately 100 mm, whereas the maximum inward displacement of 0.23 m was observed at the crown. Figure 11(b) shows crack distribution around the tunnel. In both cases, sheer cracks (black lines) were the most prevalent near the tunnel. Excavation without support exhibited higher crack density and a considerably wider crack zone than that with rock bolts, which induced more inward deformation of the tunnel. Therefore, the proposed model could simulate rock bolt functions to reinforce the rock mass and to reduce displacement around excavation. The influences of rock bolt properties on tunnel deformation are subsequently presented in the following sections.

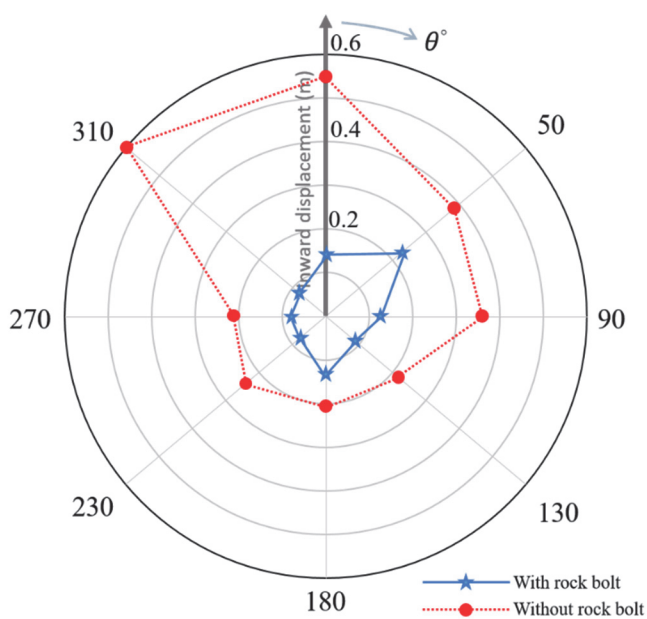### 6.3 Influence of Length of the Rock Bolt

To investigate the influence of the length of the rock bolt on tunnel deformation, this study analyzed the rock bolt system with four different lengths, which ranged from 6 ~ 14 m. In the rock bolt system, seven bolts were placed around the section, which was the same as that in Fig. 11. Figure 12 shows variations in inward displacements of the tunnel for different lengths of the rock bolt. As the length of the rock bolt increased from 6 m to 12 m, the maximum inward displacement decreased from 0.28 m to 0.22 m. The greater length of the rock bolt was positively associated with higher resistance. However, the inward displacement was almost constant until the length of the rock bolts increased to 14 m. Thus, the increasing length of the rock bolt increased the reinforced effect; however, when the length of the rock bolt increased to an upper bound value, the increase in the reinforced effect was limited. In addition, the failure type of the rock bolt may change from the cone failure to bond failure when the length of the rock bolt increased (Fig. 1).

(a) Deformation pattern

(b) Crack distribution

(c) Distribution of inward displacement around the tunnel

Fig. 11   Comparison between the two analyzed tunnel cases: excavation with and without the rock bolt support
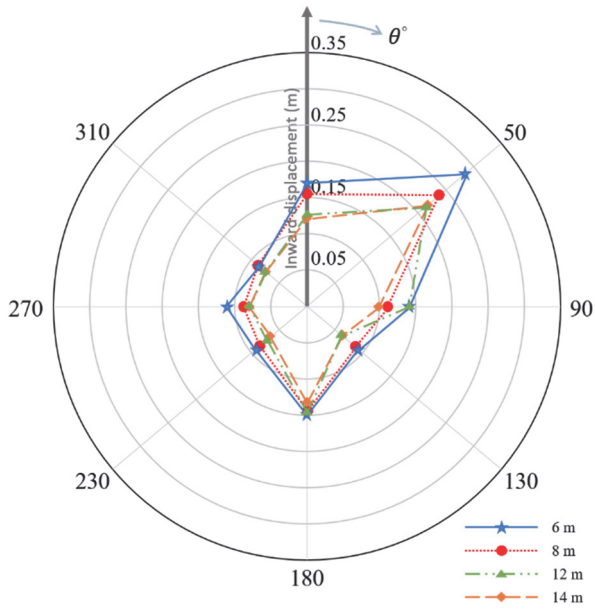
Fig. 12   Variations in inward displacements of the tunnel under different lengths of the rock bolt system

6.4   Influence of Rock Bolt Arrangement

This study further investigated the influence of the arrangement of the rock bolt on tunnel deformation, and the support system with bolts of different numbers from 7 to 13 were analyzed. The length of the rock bolts was 8 m. Figure 13 shows rock bolt arrangements around the tunnel. The rock bolts were installed at the crown and sidewalls of the tunnel. With the increasing number of bolts, the spacing between bolts decreased. Figure 14 shows distributions of inward displacements of the tunnel under different arrangements of the support system. A higher number of rock bolts were installed at the crown and sidewalls, the reinforced effect could be improved, which reduced inward displacement. With the increasing number of rock bolts from 7 to 9, the maximum inward displacement decreased from 0.24 m to 0.15 m. However, the inward displacement was almost constant when the number of rock bolts was higher than 11. The increasing number of the rock bolts increased the reinforced effect; however, when the number of rock bolts increased to an upper bound value and the spacing of rock bolt decreased to a lower bound value, the increment in the reinforced effect was limited. This group effect is similar to the pile-group effect. Due to the decrease of spacing, each bolt in a group affects the rock resistance around other bolts. A group of bolts around a section exhibit less resistance than the sum of the resistance of individual bolts.
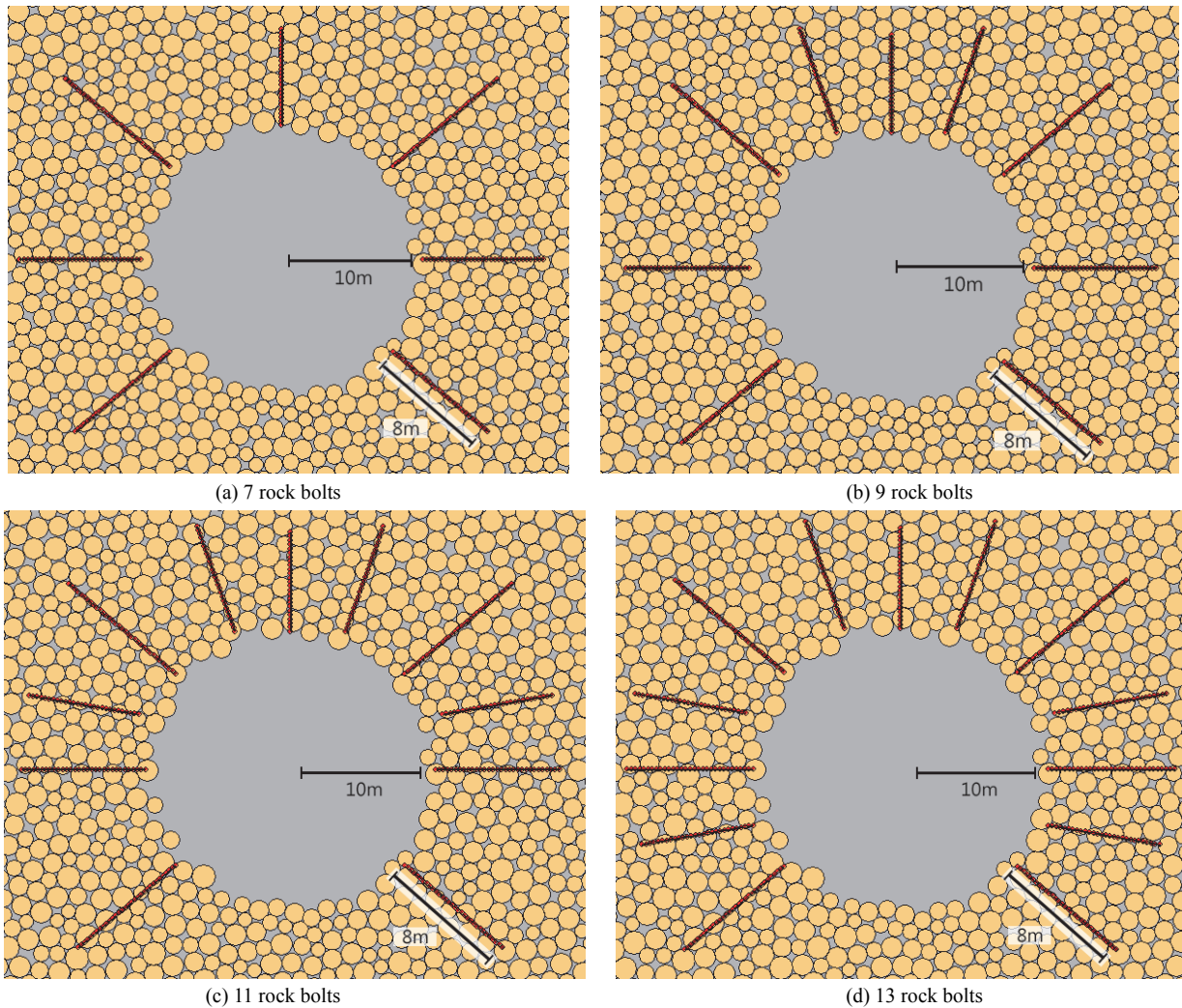

(a) 7 rock bolts

(b) 9 rock bolts

(c) 11 rock bolts

(d) 13 rock bolts

Fig. 13   Rock bolt arrangements around the tunnel for DEM analysis
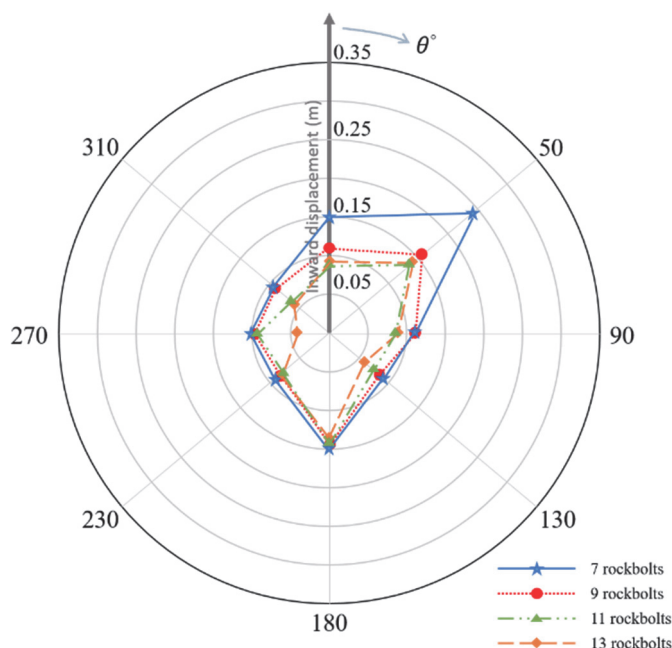
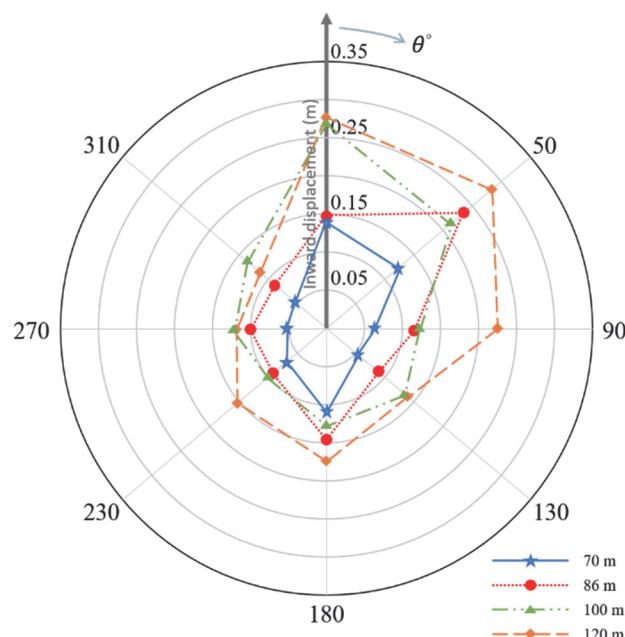**Fig. 14   Variations in inward displacements of the tunnel under different arrangements of the support system**

Fig. 15   Variations in inward displacements of the tunnel for different overburden depths

6.5   Influence of Overburden

To study the influence of overburden depth on tunnel deformation, this study analyzed the overburden depth of 70 ~ 120 m. The rock bolt system had seven bolts around the section, and the length of the bolts was 8 m, which was the same as that in Fig. 11. Figure 15 shows variations in inward displacements of the tunnel for different overburden depths. With an increasing in the overburden depth from 70 m to 120 m, the maximum inward displacement increased from 0.15 m to 0.27 m. A greater overburden depth induced higher earth pressure, thus increasing the inward displacements of the tunnel.

6.6   Influence of Rock Bolt Properties

This study further investigated the influence of interface properties of the rock bolt on tunnel deformation. In this study, three interface properties of rock bolts, namely the friction coefficient, normal stiffness, and shear stiffness, were examined. Figure 11 presents the basic analysis. Figure 16 shows variations in the inward displacements of the tunnel with different interface properties. For the effect of the interface friction coefficient (Fig. 16(a)), with the increasing friction coefficient from 0.5 to 1.83, the maximum inward displacement decreased from 0.30 m to 0.20 m. The friction coefficient of the interface significantly affected the reinforcement of the rock bolt. The effect of the interface normal stiffness was minor (Fig. 16(b)). When the normal stiffness increased from 100 MN/m^3 to 9,000 MN/m^3, inward displacement was quite closely distributed. In contrast to normal stiffness, the shear stiffness of the interface had an evident apparent effect on the rock bolt behavior (Fig. 16(c)). When the shear stiffness increased from 10 MN/m^3 to 90 MN/m^3, the maximum inward displacement decreased from 0.35 m to 0.24 m. In general, the friction coefficient and shear stiffness of the interface had a significant effect on the performance of rock bolts for the tunnel support.

7.   CONCLUSIONS

This study proposed a rock bolt model of DEM based on the specified interface concept to simulate the interaction between the bolt and rock mass. The bolt body comprised raw bonded ball elements, and the interface between the rock bolt and surrounding rock mass was simulated using the particulate interface model. DEM simulation based on the proposed model could effectively install a series of rock bolts at the specific positions to form a support system. The proposed model was verified through laboratory pull-out and shear tests. The simulation results were consistent with experimental results in terms of the force–displacement curve and failure morphology. Moreover, the primary influencing microparameters on strength and stiffness were clarified. A series of tunnel cases were further simulated to compare the difference among displacement distributions of the tunnel under different rock bolt configurations. The simulation results showed that the proposed model could simulate rock bolt functions on tunnel excavation to reinforce the rock mass and reduce displacement around excavation. Furthermore, the effects of rock bolt configurations on tunnel deformation were investigated. The increasing length and number of the rock bolt could increase the reinforced effect; however, when the length and number of the rock bolts increased to an upper bound value, the increase in the reinforced effect was limited. For the rock bolt properties, the friction coefficient and shear stiffness of the interface had a significant effect on the performance of the rock bolts for the tunnel support. The proposed model provided a useful tool to simulate rock bolt systems for tunnel engineering. However, the limitations of the proposed model should be noted. The model does not consider the pre-stressed condition of the rock bolt and cannot simulate the elastic–plastic behavior, that is, the yielding of ductile deformation. In addition, this study only develops the rock bolt supporting, and other supporting components, including shotcrete, and lining, are not considered. Further studies will focus on more types of support components and their interactions.
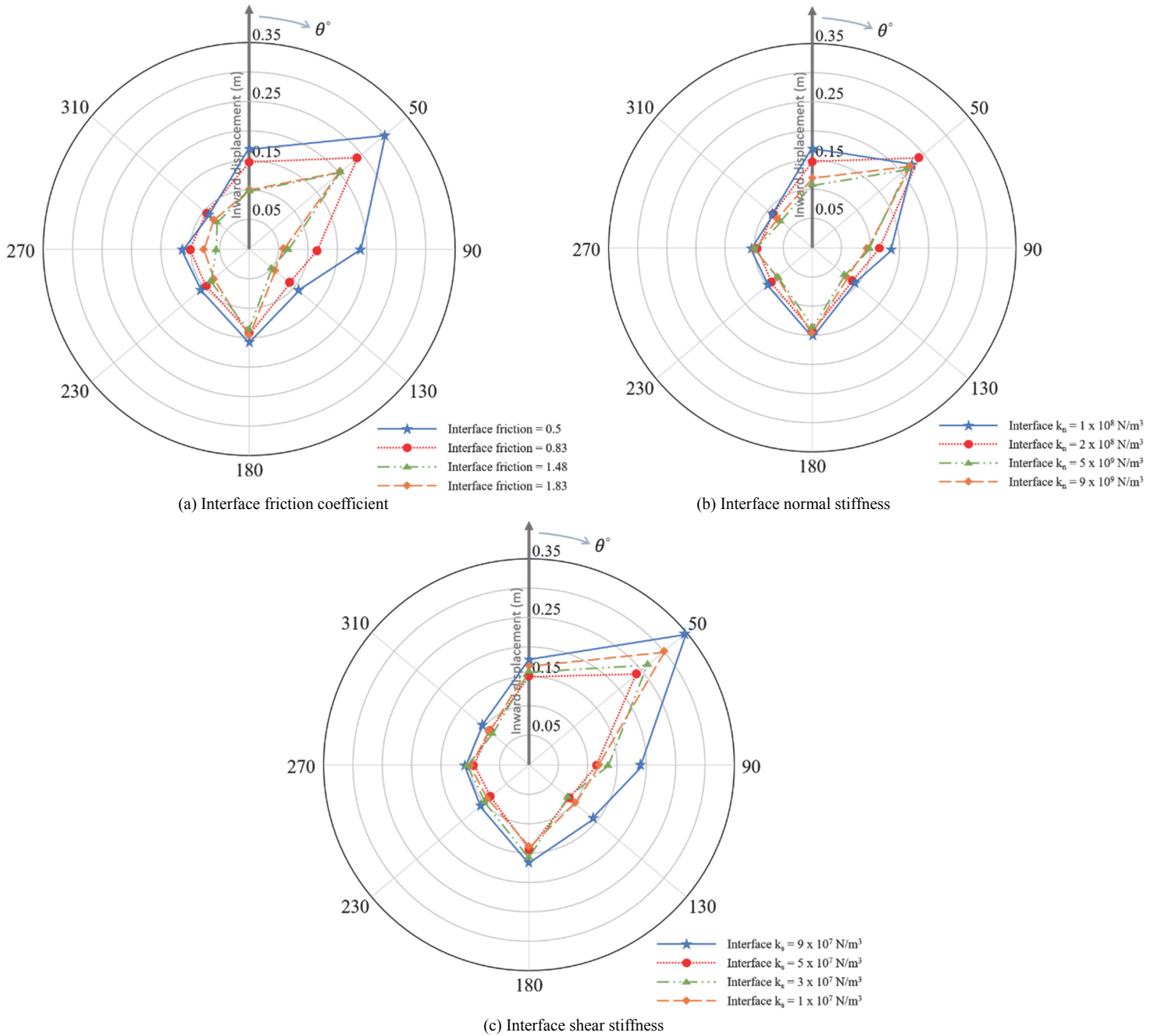
(a) Interface friction coefficient

(b) Interface normal stiffness

(c) Interface shear stiffness

Fig. 16   Variations in inward displacements of the tunnel with different interface properties

FUNDING

DATA AVAILABILITY

The data and/or computer codes used/generated in this study are available from the corresponding author on reasonable request.

CONFLICT OF INTEREST STATEMENT

The authors declare that they have no known competing financial interests or personal relationships that could have appeared to influence the work reported in this paper.

NOTATIONS

A_{sj}	Area of an interface plane (m²)
c_{sj}	Cohesion of an interface (N/m²)
$F_{n,sj}$	Normal force acting on an interface plane (N)
$\mathbf{F}_{s,sj}$	Shear force vector acting on an interface plane before force-displacement calculation (N)
$\mathbf{F}'_{s,sj}$	Shear force vector acting on an interface plane after force-displacement calculation (N)
g	Density (kg/m³)
k_n	Normal stiffness of particle (N/m)
$k_{n,sj}$	Normal stiffness of an interface (N/m³)
k_s	Shear stiffness of particle (N/m)

$k_{s,sj}$	Shear stiffness of an interface (N/m^3)
$\bar{k}_n$	Normal stiffness of parallel bond (N/m^3)
$\bar{k}_s$	Shear stiffness of parallel bond (N/m^3)
ΔU_n^e	Normal displacement in the unbonded part (m)
$\Delta \mathbf{U}_s^e$	Shear displacement vector of the interface (m)
μ	Friction coefficient of an interface

REFERENCES

Cai, Y., Esaki, T., and Jiang, Y. (2004). "An analytical model to predict axial load in grouted rock bolt for soft rock tunnelling." *Tunnelling and Underground Space Technology*, 19, 607-618. http://doi.org/10.1016/j.tust.2004.02.129

Chen, Y. (2014). "Experimental study and stress analysis of rock bolt anchorage performance." *Journal of Rock Mechanics and Geotechnical Engineering*, 6, 428-437. http://doi.org/10.1016/j.jrmge.2014.06.002

Chiu, C.C. (2010). *Using Distinct Element Method Simulating Constrain Effect of Rockbolts on Joint Dilation and Associated Mechanical Effects*. M.S. Thesis, Department of Civil Engineering, National Taiwan University. http://doi.org/10.6342/NTU.2010.01336

Chiu, C.C. and Weng, M.C. (2019a). "DEM simulation of planar sliding using a particulate interface model considering velocity-dependent friction." *Computers and Geotechnics*, 112, 51-59. http://doi.org/10.1016/j.compgeo.2019.04.001

Chiu, C.C. and Weng, M.C. (2019b). "Simulating interface characteristics by using a particulate interface model of a discrete element method." *Computers and Geotechnics*, 109, 1-11. http://doi.org/10.1016/j.compgeo.2019.01.011

Chiu, C.C., Weng, M.C., and Huang, T.H. (2015). "Biconcave bond model for cemented granular material." *Journal of Geo-Engineering*, TGS, 10, 91-103. http://doi.org/10.6310/jog.2015.10(3).3

Chiu, C.C., Weng, M.C., and Huang, T.H. (2017). "Characterization of clastic rock using a biconcave bond model of DEM." *International Journal for Numerical and Analytical Methods in Geomechanics*, 41, 422–441. http://doi.org/10.1002/nag.2568

Collins, D.M., Cook, R. A., Klingner, R.E., and Polyzois, D. (1989). *Load-Deflection Behavior of Cast-in-Place and Retrofit Concrete Anchors Subjected to Static, Fatigue, and Impact Tensile Loads*. Research Report No. 1126-1, Center for Transportation Res., Univ. of Texas, Austin, Texas.

Cook, R. (1993). "Behavior of chemically bonded anchors." *Journal of Structural Engineering*, ASCE, 119, 2744-2762. http://doi.org/10.1061/(ASCE)0733-9445(1993)119:9(2744)

Itasca Consulting Group, Inc. (2014). *PFC — Particle Flow Code*, Ver. 4.0. Minneapolis: Itasca.

Li, C. and Stillborg, B. (1999). "Analytical models for rock bolts." *International Journal of Rock Mechanics and Mining Sciences*, 36, 1013-1029. http://doi.org/10.1016/S1365-1609(99)00064-7

Lin, C.H., Li, H.H., and Weng, M.C. (2018). "Discrete element simulation of the dynamic response of a dip slope under shaking table tests." *Engineering Geology*, 243, 168-180. http://doi.org/10.1016/j.enggeo.2018.07.005

Luke, P.C.C., Chon, C., and Jirsa, J.O. (1985). *Use of Epoxies for Grouting Reinforcing Bar Dowels in Concrete*. PMFSEL Report No. 85-2, Phil M. Ferguson Structural Engineering Lab., Dept. of Civ. Engrg., Bureau of Engrg. Res., The Univ. of Texas, Austin, Texas.

Potyondy, D.O. and Cundall, P.A. (2004). "A bonded-particle model for rock." *International Journal of Rock Mechanics and Mining Sciences*, 41, 1329-1364. http://doi.org/10.1016/j.ijrmms.2004.09.011

Spang, K. (1988). Thèse: Beitrag zur rechnerischen Berficksichtung vollvermörtelter Anker bei der Sicherung von Felsbauwerken in geschichtetem oder geklfiftetem Gebirge.

Spang, K. and Egger, P. (1990). "Action of fully-grouted bolts in jointed rock and factors of influence." *Rock Mechanics and Rock Engineering*, 23, 201-229. http://doi.org/10.1007/BF01022954

Thenevin, I., Blanco-Martín, L., Hadj-Hassen, F., Schleifer, J., Lubosik, Z., and Wrana, A. (2017). "Laboratory pull-out tests on fully grouted rock bolts and cable bolts: Results and lessons learned." *Journal of Rock Mechanics and Geotechnical Engineering*, 9, 843-855. http://doi.org/10.1016/j.jrmge.2017.04.005

Weng, M.C., Lo, C.M., Wu, C.H., and Chuang, T.F. (2015). "Gravitational deformation mechanisms of slate slopes revealed by model tests and discrete element analysis." *Engineering Geology*, 189, 116-132. http://doi.org/10.1016/j.enggeo.2015.01.024

Weng, M.C., Jeng, F.S., Hsieh, Y.M., Huang, T.H. (2008). "A simple model for stress-induced anisotropic softening of weak sandstones." *International Journal of Rock Mechanics and Mining Sciences*, 45, 155-166. http://doi.org/10.1016/j.ijrmms.2007.04.004

Weng, M.C., Tsai, L.S., Liao, C.Y., and Jeng, F.S. (2010). "Numerical modeling of tunnel excavation in weak sandstone using a time-dependent anisotropic degradation model." *Tunnelling and Underground Space Technology*, 25, 397-406. http://doi.org/10.1016/J.TUST.2010.02.004

Weng, M.C., Chen, T.C., and Tsai, S.J. (2017). "Modeling scale effects on consequent slope deformation by centrifuge model tests and the discrete element method." *Landslides*, 14, 981-993. http://doi.org/10.1007/s10346-016-0774-7

Wu, S. and Xu, X. (2016). "A study of three intrinsic problems of the classic discrete element method using flat-joint model." *Rock Mechanics and Rock Engineering*, 49, 1813-1830. http://doi.org/10.1007/s00603-015-0890-z